Pergamon

*Journal of Atmospheric and Terrestrial Physics*, Vol. 56, No. 10, pp. 1237–1249, 1994

0021-9169/94 $7.00 + 0.00

# Semidiurnal tide in the 80–150 km region: an assimilative data analysis

J. M. FORBES,*††† A. H. MANSON,† R. A. VINCENT,‡ G. J. FRASER,§ F. VIAL,‖ R. WAND,¶ S. K. AVERY,** R. R. CLARK,†† R. JOHNSON,‡‡ R. ROPER,§§ R. SCHMINDER,‖‖ T. TSUDA¶¶ and E. S. KAZIMIROVSKY***

*High Altitude Observatory, National Center for Atmospheric Research, Boulder, CO 80303-3000, U.S.A.; †Institute for Space and Atmospheric Studies, University of Saskatchewan, Saskatoon, Canada; ‡Department of Physics, University of Adelaide, Adelaide, SA, Australia; §Department of Physics, University of Canterbury, Christchurch, New Zealand; ‖Laboratoire de Meteorologie Dynamique du CNRS, Ecole Polytechnique, Palaiseau, France; ¶MIT Haystack Observatory, Westford, Massachusetts, U.S.A. (formerly affiliated with); **Department of Electrical and Computer Engineering, University of Colorado, U.S.A.; ††Department of Electrical and Computer Engineering, University of New Hampshire, U.S.A.; ‡‡Space Physics Research Laboratory, University of Michigan, Ann Arbor, Michigan, U.S.A.; §§School of Earth and Atmospheric Sciences, Georgia Institute of Technology, Atlanta, Georgia, U.S.A.; ‖‖Collm Geophysical Observatory, University of Leipzig, Collm, Germany; ¶¶Radio Atmospheric Science Center, Kyoto University, Japan; ***Siberian Institute of Terrestrial Magnetism, Ionosphere and Radio Propagation, Irkutsk, C.I.S.

(*Received in final form* 15 *June* 1993; *accepted* 1 *July* 1993)

**Abstract**—A set of tabulated functions called 'Hough Mode Extensions' (HMEs), which represent numerical extensions of classical Hough modes into the viscous regime of the thermosphere, are used to least-squares fit a climatological data base of tidal measurements. The data base consists of monthly average vertical profiles of semidiurnal amplitudes and phases at 17 radar sites accessing some part of the 80–150 km height region. The radars are distributed between 78° S and 70° N latitude, and each one provides measurements of one or more of the following: eastward wind, southward wind, perturbation temperature. As a result of the fitting process, a single complex normalizing coefficient is derived for each month and for each of the four HMEs, designated (2,2), (2,3), (2,4) and (2,5) after their classical Hough function designations. Once the complex coefficients are derived, reconstruction by weighted superposition of the HMEs results in globally continuous specifications of semidiurnal horizontal and vertical wind, temperature, pressure, and density throughout the 80–150 km height region. The tidal variations in density, in particular, provide greater accuracy for several aerospace applications. The methodology developed here can also be utilized to derive tidal lower boundary conditions for Thermospheric General Circulation Models (TGCMs), or as a basis for future empirical model development. Comparisons are also made with HME coefficients and global tidal fields from the FORBES and VIAL [(1989) *J. atmos. terr. Phys.* **51**, 649] numerical tidal model.

## 1. INTRODUCTION

The semidiurnal tide in the upper mesosphere and lower thermosphere (c. 80–130 km) has been studied for several decades, mainly through analyses of winds and temperatures measured by meteor, spaced antenna drift, and incoherent scatter radars. However, only recently have multi-station measurements been organized and examined to elucidate global climatological features on a month-by-month basis [see Atmospheric Tides Middle Atmosphere Program (ATMAP) Special Issue of the *Journal of Atmospheric and Terrestrial Physics*, July/August 1989, notably papers by AVERY *et al.* (1989), MANSON *et al.* (1989), VINCENT *et al.* (1989), SCHMINDER *et al.* (1989) and KAZIMIROVSKY and ZHOVTY (1989)]. These observational advances, along with those making available monthly specifications of zonally averaged winds and temperatures throughout the middle atmosphere (LABITZKE *et al.*, 1985), have sparked numerical simulations delineating the latitudinal and vertical structures of tidal oscillations for each month of the year (FORBES and VIAL, 1989).

Due to assumptions made in parameterizing the second-order derivatives associated with diffusion of heat and momentum by linear damping terms, the

†††Permanent affiliation: Department of Aerospace Engineering Sciences, University of Colorado, Boulder, CO, U.S.A.

FORBES and VIAL (1989) results are subject to increasing error above 100 km. In order to provide a more accurate theoretical estimate of tidal oscillations in the 100–150 km region for comparison with incoherent scatter radar data, FORBES and VIAL (1991) utilized the methodology of FORBES and HAGAN (1982) to extend the FORBES and VIAL (1989) tidal solutions into the viscous regime above 100 km. Briefly, FORBES and HAGAN (1982) and FORBES *et al.* (1982) describe and tabulate normalized solutions to the linear thermospheric tidal equations on a spherical Earth that define extensions into the thermosphere of self-consistent wind and temperature structures associated with the (2,2), (2,3), (2,4), and (2,5) semidiurnal tidal modes. Molecular diffusion of heat and momentum is accounted for by the full second derivative terms with respect to height. The tabulations extend from 80 to 400 km and cover five levels of solar activity, corresponding to global mean exospheric temperatures of 600, 800, 1000, 1200 and 1400 K. FORBES and VIAL (1991) utilized the HME structures in their analysis as follows. For each month of the year, the perturbation temperatures calculated by FORBES and VIAL (1989) at 100 km were decomposed into Hough functions. The coefficients of this expansion were then used to calibrate the (2,2), (2,3), (2,4), and (2,5) Hough Mode Extensions (HMEs) into the thermosphere of these classical modes. The summation of appropriately calibrated HMEs, along with a relatively small *in situ* contribution (FORBES, 1982a,b), thus provided monthly global specifications of semidiurnal winds, temperatures, and densities up to about 150 km which are consistent with FORBES and VIAL (1989) below 100 km. FORBES and VIAL (1991) compared these theoretical predictions with seasonal mean tidal temperatures and winds in the *E*-region derived from measurements taken at the Arecibo, Millstone Hill and Chatanika incoherent scatter radar facilities.

FORBES and SALAH (1991) utilized the HME structures in a different but complementary fashion. Their work focuses on the mesosphere–thermosphere coupling due to the solar semidiurnal atmospheric tide during the first Lower Thermosphere Coupling Study (LTCS) campaign interval of 21–25 September 1987. During this period, determinations of semidiurnal eastward ($u$) and southward ($v$) velocity components and temperature ($\delta T$) were available within the 80–150-km region from a total of 13 incoherent scatter, meteor, and spaced antenna drift radars. Using the FORBES and HAGAN (1982) set of numerically generated HME functions for $u$, $v$ and $\delta T$ corresponding to the (2,2), (2,3), (2,4) and (2,5) semidiurnal tidal modes, a least-squares fit to the radar data was performed. The fit results in a single (complex) normalizing factor for each HME from which globally continuous and internally consistent semidiurnal oscillations in $u$, $v$ and $\delta T$ (as well as vertical velocity and density) can be derived.

A difficulty with the FORBES and SALAH (1991) analysis is that the observed oscillations with 12-h periodicity contain an element of day-to-day variability; this might represent the presence of local contributions to spectral energy around the 12-h peak which would not be well correlated between stations, and would not be amenable to representation by global fitting functions. In the present paper, we seek to perform the same exercise as in FORBES and SALAH (1991), utilizing instead monthly climatological data from a global array of stations. For each month, a single complex coefficient is derived corresponding to each semidiurnal HME, which are nearly indistinguishable from classical Hough modes at 100 km. Comparison with a Hough mode decomposition of the FORBES and VIAL (1989) numerical model results at 100 km provides a very concise means of comparing the monthly progressions of amplitudes and phases of the complex normalizing coefficients derived by both methods. Alternatively, global tidal fields can be generated and intercompared.

The least-squares fitting procedure is reviewed briefly in Section 3. In Section 4 results of the numerical analysis and comparison with the coefficients and global tidal fields corresponding to the FORBES and VIAL (1989) theoretical model are presented. Section 5 is reserved for concluding remarks. In the section following, the radar data base is described.

## 2. DATA BASE

The data used in the present study are described in Table 1. Listed are the station names, locations, averaging periods, height ranges of usable semidiurnal data and parameters measured ($u$ = eastward wind, $v$ = southward wind, and $\delta T$ = temperature). Only data above 80 km and below 130 km were utilized in the fitting process, the former constraint being set by the limit of tabulated HMEs, and the latter in order to minimize the contribution of the *in situ* generated semidiurnal tide (FORBES and SALAH, 1991). Two of the stations in Table 1 (Collm and Atlanta) are marked with an asterisk. These data were not included in the fitting process, but are used for an independent comparison with the empirically reconstructed tidal fields. This reconstruction process is described in Section 3, and the data comparisons are presented in Section 4.

Most of the climatological data originating from the

Table 1. Data base

| Station name | Location | Years | Heights (km) | Measured |
|---|---|---|---|---|
| Tromsø, Norway | (70° N, 19° E) | May 1987–July 1989 | 61–112 | $u, v$ |
| Poker Flat, Alaska | (65° N, 147° W) | 1983–1984 | 75–106 | $u, v$ |
| Chatanika, Alaska | (65° N, 148° W) | 1976–1981 | 90–130 | $u, v$ |
| Saskatoon, Canada | (52° N, 107° W) | 1985 | 61–112 | $u, v$ |
| Badary, C.I.S. | (52° N, 120° E) | 1976–1986 | ~95 | $u, v$ |
| Collm, Germany* | (52° N, 15° E) | 1983–1986 | 88–110 | $u, v$ |
| Garchy, France | (47° N, 3° E) | 1970–1976 | 78–102 | $u$ |
| Monpazier, France | (44° N, 1° E) | 1976–1980 | 78–102 | $u$ |
| Durham, New Hampshire | (43° N, 71° W) | 1978–1984 | 77–110 | $u, v$ |
| Millstone Hill, Massachusetts | (43° N, 72° W) | 1976–1977 | 100–140 | $u, v$ |
| | | 1970–1975 | 100–140 | $\delta T$ |
| Kyoto, Japan | (35° N, 136° E) | 1983–1985 | 82–106 | $u, v$ |
| Atlanta, Georgia* | (34° N, 84° W) | 1983–1984 | 80–100 | $u, v$ |
| Arecibo, Puerto Rico | (18° N, 67° W) | 1966–1975 | 100–140 | $\delta T$ |
| Townesville, Australia | (18° S, 147° E) | 1978–1980 | 80–98 | $u, v$ |
| Adelaide, South Australia | (35° S, 138° E) | 1984–1986 | 78–98 | $u, v$ |
| Christchurch, New Zealand | (44° S, 173° E) | June 1978–Feburary 1980 | 65–103 | $u, v$ |
| Mawson, Antartica | (68° S, 63° E) | June 1984–1986 | 80–108 | $u, v$ |
| Scott Base | (78° S, 170° E) | December 1982–November 1984 | 81–97 | $u, v$ |

radars accessing the region between c. 70 and 110 km are the same as those presented in the ATMAP special issue of the *Journal of Atmospheric and Terrestrial Physics* (July/August, 1989), with some updating for particular sites (Tromsø, Scott Base). Hereafter we will refer to these as the 'MLT' (mesosphere/lower thermosphere) radars. The MANSON *et al.* (1989) paper of that special issue describes the data from Saskatoon, Collm, Garchy, Monpazier, Durham and Christchurch. The Poker Flat, Tromsø, Mawson and Scott Base data are described in AVERY *et al.* (1989). The comparison of Adelaide and Kyoto climatologies is given in VINCENT *et al.* (1989), and the Badary data are described in KAZIMIROVSKY and ZHOVTY (1989).

The data base also includes incoherent scatter (IS) determinations of neutral temperatures and winds in the 90–150 km region. Due to the sparsity of data in this region, seasonal averages from the Arecibo, Millstone Hill and Chatanika radars as described in FORBES and VIAL (1991) are utilized here. The Chatanika data, which cover only the summer season, originate from JOHNSON *et al.* (1987). The Millstone and Arecibo data are largely described in WAND (1976, 1983a,b,c), WAND and HARPER (1978), and WAND and SALAH (1978). The Arecibo *E*-region neutral temperatures were reanalyzed by FORBES and VIAL (1991) and are described therein.

A shortcoming of the data base described in Table 1 is that the averaging periods differ from station to station, and hence there is some degree of interannual variability which will tend to introduce a level of uncertainty in the final results. However, in virtually all of the studies cited above, and in other analyses of long-term data sets which are not included in the present data base, there are certain salient characteristics of the vertical tidal structures, during any given month, which tend to repeat themselves from year to year for a particular station or grouping of stations. These are primarily the features which remain after averaging over several years, and which we strive to capture with the HME fitting process. We have, in the present study, chosen to work with a data set which represents a wide range of latitudes and encompasses a wider altitude regime, in lieu of a much more geographically limited but temporally consistent data set which would provide inadequate constraints in the fitting process. FORBES and SALAH (1991) use a mock data base from a numerical tidal model to demonstrate the importance of southern hemisphere and *E*-region measurements in complementing northern hemisphere data below 100 km to ensure a robust fit.

On the average, for each month, approximately 300–350 independent observations (i.e. $u$, $v$ or $\delta T$ at a given height for each station) were available for each fit.

## 3. FITTING AND RECONSTRUCTION PROCEDURES

The fitting procedure is identical to the one described in some detail by FORBES and SALAH (1991), and is only briefly outlined here. Basically, we utilize

the method of multiple linear regression to fit the observational data (in a least-squares sense) to the thermospheric extensions (HMEs) of the classical expansion functions corresponding to the (2,2), (2,3), (2,4), and (2,5) semidiurnal tidal modes as reported by FORBES and HAGAN (1982) and tabulated by FORBES *et al.* (1982). Above 100 km the combined effects of rotation and viscous dissipation introduce changes with height of the horizontal shapes, or equivalently, changes with latitude of the vertical structures, of the HMEs as compared with classical tidal functions. Sample plots illustrating the main features are provided in FORBES and SALAH (1991), in addition to the more extensive illustrations in FORBES and HAGAN (1982) and FORBES *et al.* (1982).

The HME functions tabulated by FORBES *et al.* (1982) are normalized to a temperature amplitude of unity and phase of 0600 LT at an altitude of 100 km, at specific latitudes for each mode: (2,2), 0°; (2,3), 24°; (2,4), 36°; and (2,5), 42°. As first noted by LINDZEN *et al.* (1977), it is important to emphasize that for each mode there exist unique latitude and height structures for temperature, vertical velocity, eastward velocity, southward velocity, density and pressure which must remain internally consistent; that is, for a given HME all amplitudes are arbitrary to within a single constant factor (appropriate to all fields at all latitudes and altitudes) while phases are arbitrary to within a single constant phase displacement. The problem can be reduced to finding a single complex normalizing factor (CNF) for each mode which leads to a satisfactory least-squares fit of any number of semidiurnal wind and temperature observations in the 80–130 km height region.

Once the complex normalizing factors for the HMEs are determined by the above procedure, it is possible by reconstruction to obtain a globally continuous empirical description of the semidiurnal tidal fields, including horizontal and vertical wind components, temperature, density and pressure. In so doing, however, one must be cognizant of the relative importance of *in situ* tidal conditions. These are generally negligible between 80 and 130 km (FORBES, 1982a,b), as they must be if our fitting procedure is to be valid. However, between 130 and 150 km a small correction is required. We account for the relatively small *in situ* contribution by adding the *in situ* component of the tidal fields from the FORBES (1982a,b) model. This allows us to extend the model to the upper levels within which standard *E*-region methods of deriving temperatures and winds from incoherent scatter radar data are valid.

## 4. RESULTS

### 4.1. *HME amplitudes and phases vs. month*

A very succinct means exists for comparing the global numerical results of FORBES and VIAL (1989, 1991) with the complete data base described in Table 1. This is accomplished through examination of the

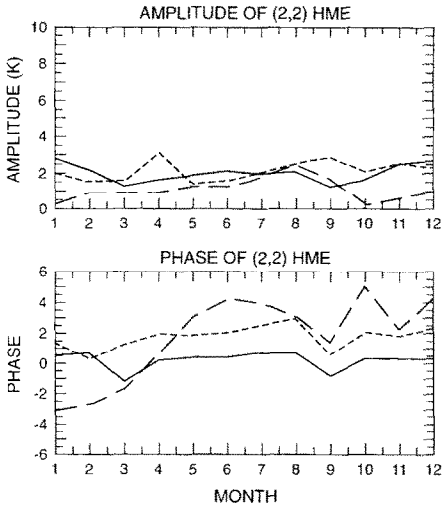


Fig. 1. Amplitude (top) and phase (bottom) of the (2,2) HME complex normalizing coefficient (CNF) vs. month at 100 km. Phase represents time of maximum amplitude in hours from local midnight. The solid line represents the FORBES and VIAL (1989, 1991) numerical model. The long-dashed line corresponds to the fit to MLT and IS radar data, and the short-dashed line corresponds to fitting only MLT radar data.

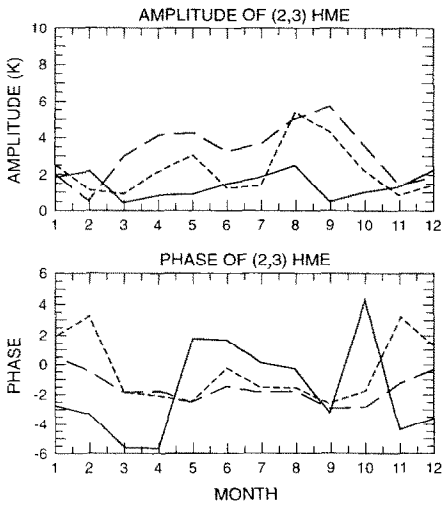


Fig. 2. Same as Fig. 1, except for (2,3) HME.

monthly progression of amplitudes and phases of the four HME CNFs as illustrated in Figs 1–4. In these figures the solid lines result from the Hough decomposition of the temperature field as calculated at 100 km in FORBES and VIAL (1989). The long-dashed curve represents the CNFs obtained from least-squares fitting the entire data base described in Table 1 (except for asterisked stations), including both MLT and IS radars. The short-dashed curve represents those CNFs derived from fitting only the MLT radar data (i.e. the *E*-region IS data from Millstone Hill, Arecibo and Chatanika are omitted from the fit). Hereafter, these results will be referred to as FV89, MLTIS, and MLT, respectively.

In Fig. 1 the amplitudes and phases of the (2,2) HMEs are compared. The FV89 amplitudes oscillate about a value of 2.0 K, dipping to minima of order 1.3 K during the equinoctial months, and achieving maxima of the order of 2.7 K during the December/January solstice. The MLT curve similarly oscillates about a value near 2.0 K, except that maxima (of the order of 2.5–3.0 K) appear near the equinoxes, rather than the minima depicted by FV89. It is at these maxima (April and September) that the two curves differ most markedly. Addition of the IS radar data to the fit (MLTIS curve) tends to reduce amplitudes for the (2,2) HME (in comparison to the MLT case), and similarly falls below the FV89 values for 10 out of 12 months. The (2,2) HME phase is about 0000 h for FV89 during most of the year, only changing to 2300 h for the equinoctial months. The MLT curve parallels the FV89 values, reflecting a phase lag of about 2 h. The MLTIS curve is generally within 3 h of MLT and FV89, but exhibits significantly more variation during the course of the year.

The (2,3) HMEs are depicted in Fig. 2. The FV89 values generally fall between 0.5 and 2.5 K, with the minima occurring at the equinoxes, and maxima during July/August and December–February. Such seasonal behavior is expected for the antisymmetric modes. The MLT and MLTIS curves, however, depict a much more intense (2,3) with maxima of 4.4 and 5.9 K during April/May and August/September for MLTIS, and maxima of 3.1 K during May and 5.4 K during August for MLT. Thus, the main antisymmetric mode appears to assume greatest importance (insofar as the data are concerned) in early and late northern hemisphere summer, instead of midsolsticial periods as one would intuitively expect, and closer to what is predicted by theory (FV89). The phase curves in Fig. 2 exhibit very good agreement between MLT and MLTIS throughout the year, but with significant departures from FV89 (of the order of 3–6 h) during at least 6 out of 12 months.

The (2,4) HMEs are illustrated in Fig. 3. The MLT and MLTIS curves again exhibit very similar features, with weak maxima of the order of 2.5–3.5 K during the equinox months and during December. The FV89 values, however, are significantly different from those obtained from the fitting process during January–April (amplitudes ranging from 4.0 to 9.3 K) and October/November (amplitudes of the order of 4–6 K). The three (2,4) HME phase curves are all in reasonably good agreement in so far as gross annual features are concerned. The FV89 curves are closer to what one intuitively expects for antisymmetric mode

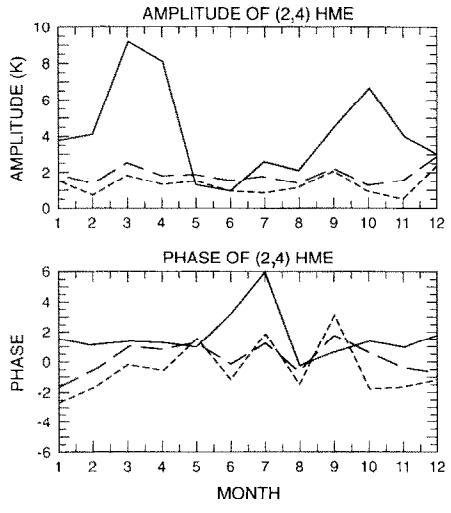


Fig. 3. Same as Fig. 1, except for (2,4) HME.

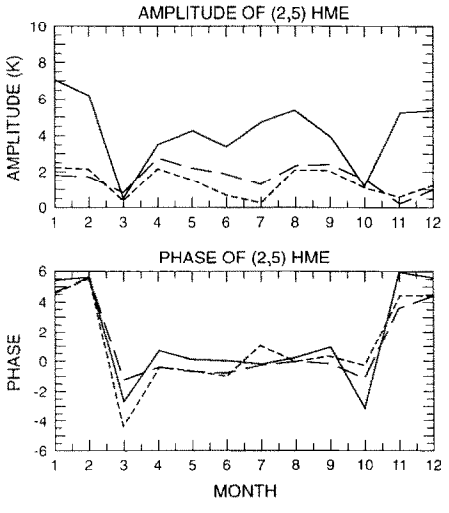


Fig. 4. Same as Fig. 1, except for (2,5) HME.

behavior: a 6-h reversal of phase around the equinoxes. The data suggest a fairly constant phase between March and September, with a shift of only 2–4 h during northern hemisphere winter.

As depicted in Fig. 4, the (2,5) HME amplitudes for FV89 again exceed those derived from the HME fitting process, achieving amplitudes of the order of 4–7 K, except during the deep minima (0.5–1.0 K) during March and October. The FV89 curve envelopes those for MLT and MLTIS, but sometimes the amplitude differences are as great as 4–5 K. By contrast, the monthly variations of phase for all three curves are in excellent agreement, and exhibit the expected 6-month phase shift around the equinoxes.

In summary, the MLT and MLTIS curves exhibit similar amplitude and phase variations throughout the year, being more similar to each other than individually to the FV89 model curve. In the case of the (2,4) and (2,5) HMEs, where significant departures exist between model and data amplitude curves, it is the model that has the higher amplitudes. On the other hand, the data suggest the presence of a much larger (2,3) mode than FV89. For all four HMEs, there is generally good phase agreement in the sense that all curves tend to fall within the same phase quadrant more often than not. Given their general phase coherence, one might expect the FV89 model to exhibit similar height/monthly/latitudinal structures as the

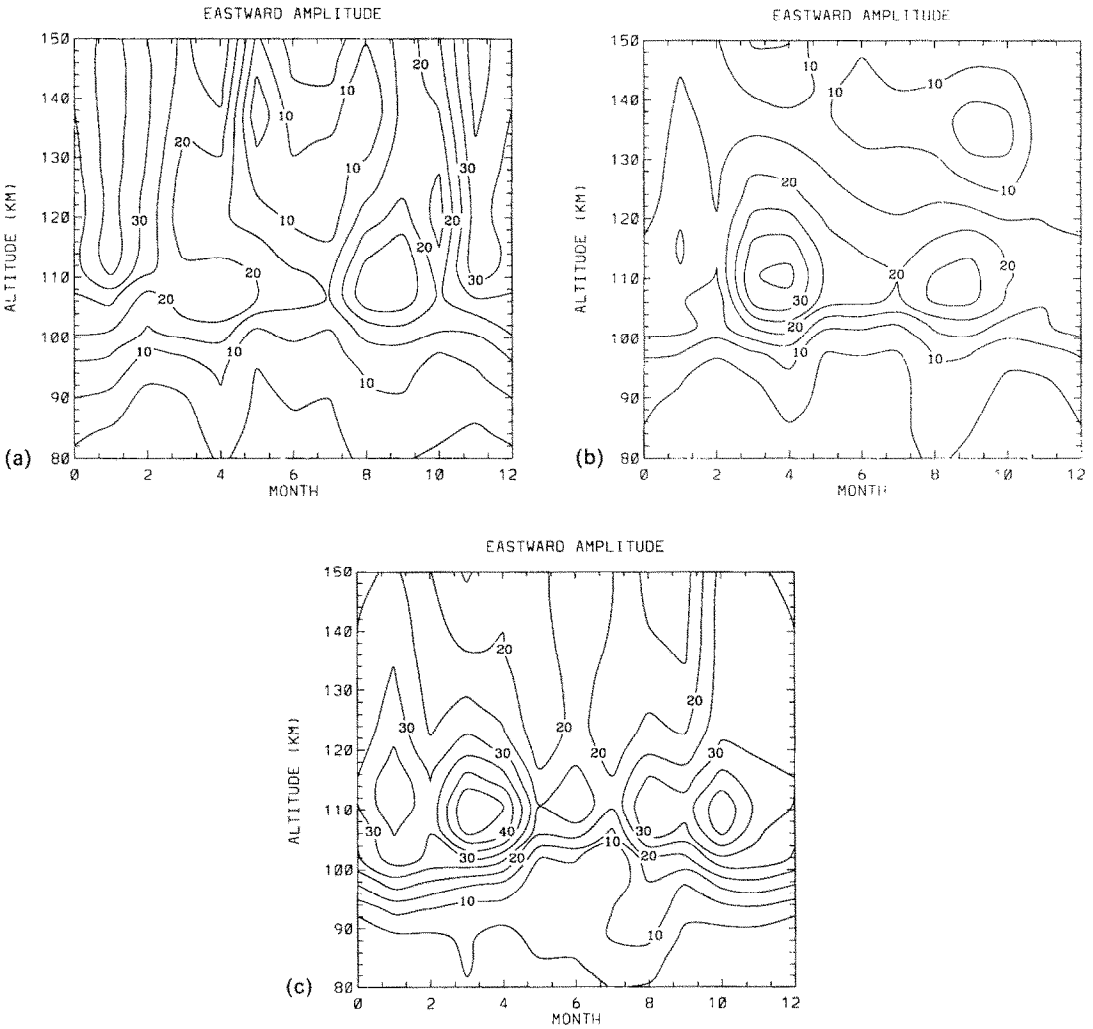


Fig. 5. Height vs. month contours for amplitude of semidiurnal eastward wind at 42° latitude. Contour spacing is 5 m/s. (a) MLT data; (b) MLT and IS data; (c) FV89 model.

empirically derived results, with generally larger amplitudes than the empirical ones. We will now examine such structures as the next step in our intercomparison between these different types of models.

### 4.2. *Comparisons of tidal fields*

In Fig. 5 we compare the height vs. month contours of the eastward semidiurnal wind amplitude at 42° latitude for the cases MLT, MLTIS and FV89 defined previously. We see that the addition of the IS radar data to the fit (MLTIS as compared with MLT) increases significantly the spring maximum in amplitude between 100 and 125 km, but diminishes the November–February maximum above 110 km. Note that minima in the MLTIS amplitudes occur during winter (November–February) and also during midsummer (June/July). Similar structures and amplitudes are predicted by the FORBES and VIAL (1989, 1991) model results [FV89; Fig. 5(c)].

A similar comparison, also at 42° latitude, is made in Fig. 6 with respect to the perturbation densities. It is significant to note that these densities are predicted primarily on the basis of wind measurements and the internal consistency of the theoretical HMEs; no density measurements were used in the construction of Fig. 6, and in fact there are very few density measurements in this height regime from which tidal oscillations can be derived. Again, the addition of

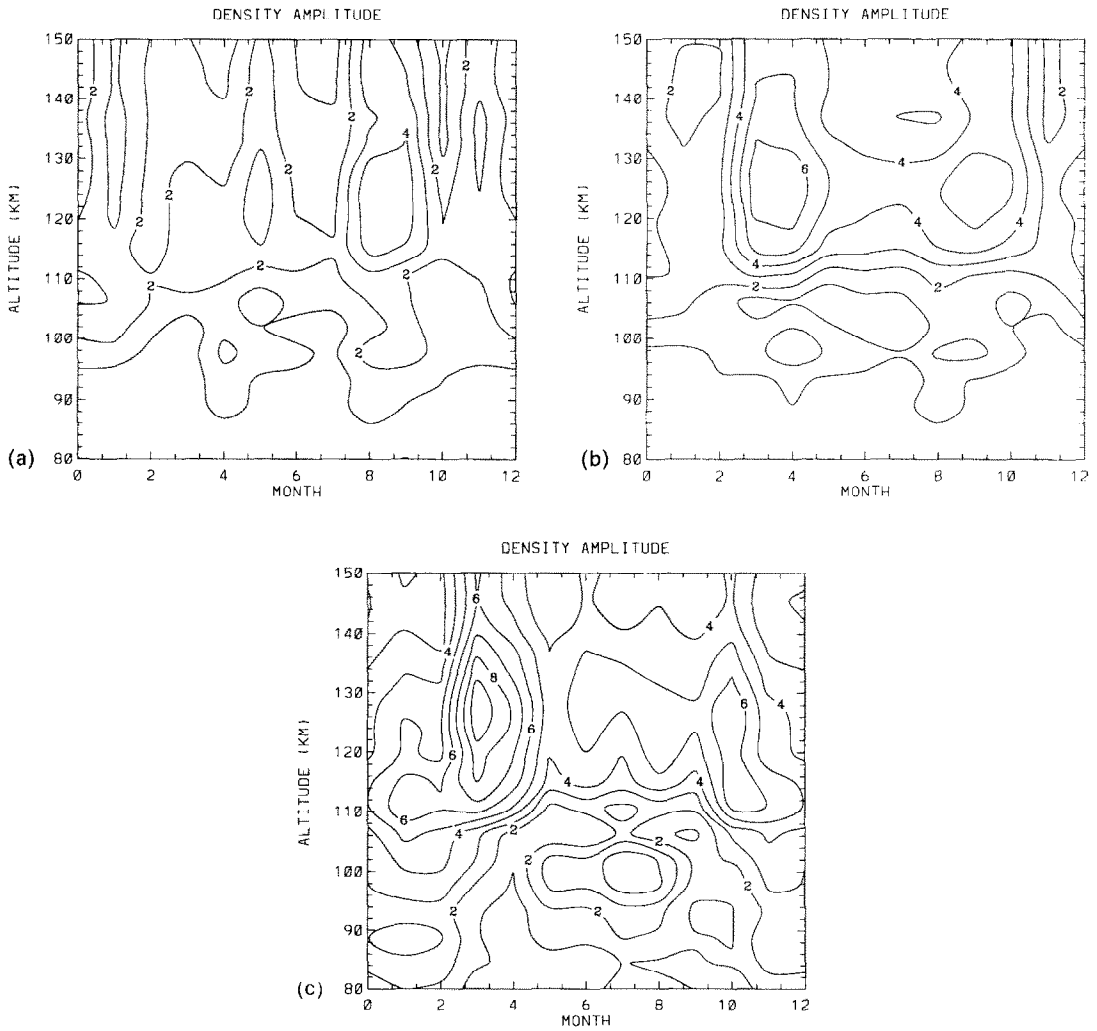


Fig. 6. Height vs. month contours for amplitude (in percent) of semidiurnal perturbation density at 42° latitude. Contour spacing is 1%. (a) MLT data; (b) MLT and IS data; (c) FV89 model.

the IS radar data to the fitting process introduces significant modifications to the $E$-region density structures, and brings the contours into much closer agreement with the FV89 results, which share many features with the MLTIS contours. A notable feature is the 6–8% density amplitude around March. This consistency serves to support the credibility of the HME fitting process as well as the realism of the FORBES and VIAL (1989, 1991) model.

The MLT, MLTIS and FV89 density phases at 42° latitude are intercompared in the height vs. month contour format in Fig. 7. The agreement is less striking than in Fig. 6, partially due to the difficulties of contouring phases in two dimensions. However, close examination reveals that where the density perturbations are greater than about 1%, phase differences between FV89 and MLTIS are generally no more than 2 h. Moreover, the vertical spacing of the contours, in other words the vertical wavelength of the tidal oscillation, is comparable for both empirical and theoretical model results.

In Fig. 8, we present the height vs. latitude contours of the southward semidiurnal wind amplitude during December for the MLT, MLTIS and FV89 cases. The corresponding phase contours are given in Fig. 9. The jet-like maxima apparent in FV89 tend to intensify and become more well-defined when the IS radar data are added to the fit (MLTIS as compared to MLT).

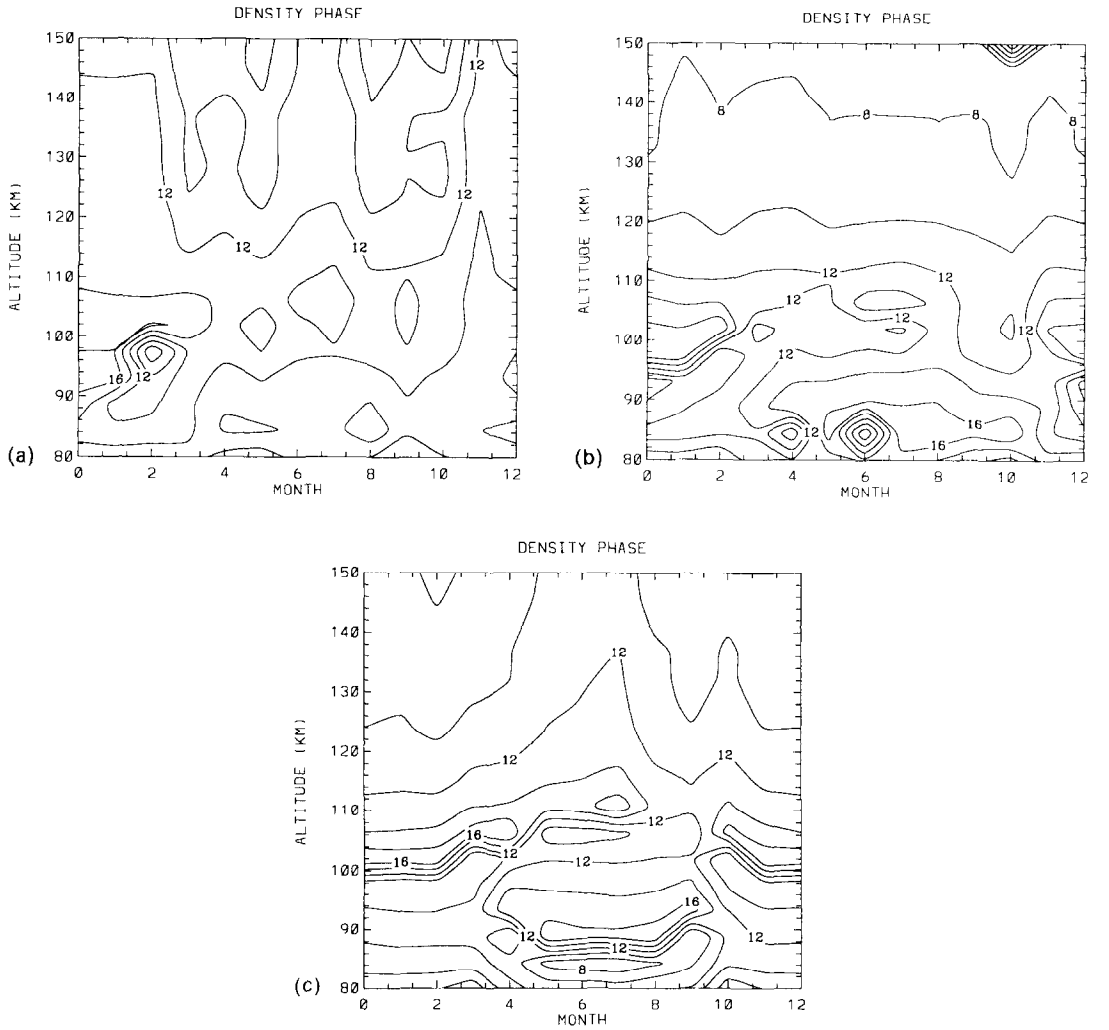


Fig. 7. Height vs. month contours for phase (local time of maximum) of semidiurnal perturbation density at 42° latitude. Contour spacing is 2 h. (a) MLT data; (b) MLT and IS data; (c) FV89 model.

The jet maxima in FV89 generally occur at higher latitudes and at lower altitudes than MLTIS, with amplitudes about a factor of two higher. These deficiencies are due in part to the lack of high-latitude *E*-region measurements in the present data base for non-summer months, and the significantly larger (2,5) amplitudes in FV89 (cf. Fig. 4) during December. The phase contours are in generally good agreement between the three cases. For instance the 10.0 h phase contour for the northern hemisphere is similarly situated in all three cases, and the vertical wavelengths are comparable. The greatest differences between MLTIS and FV89 occur in the southern hemisphere above 100 km, where there are no data. The more complex phase structure near the equator is introduced by the symmetric modes which undergo 180° phase jumps at 0° latitude.

### 4.2. *Comparisons with independent measurements*

At this point it seems reasonable to provide some measure of the quality of fit to the experimental data, and also to provide some comparisons with independent data, i.e. those which were not utilized in the fitting process. For an altitude of 90 km and latitude of 36°, Fig. 10 compares amplitudes and phases for the eastward semidiurnal wind component from the following sources: (a) FV89; (b) MLTIS; (c) Kyoto, Japan; and (d) Atlanta, Georgia, U.S.A. Details of

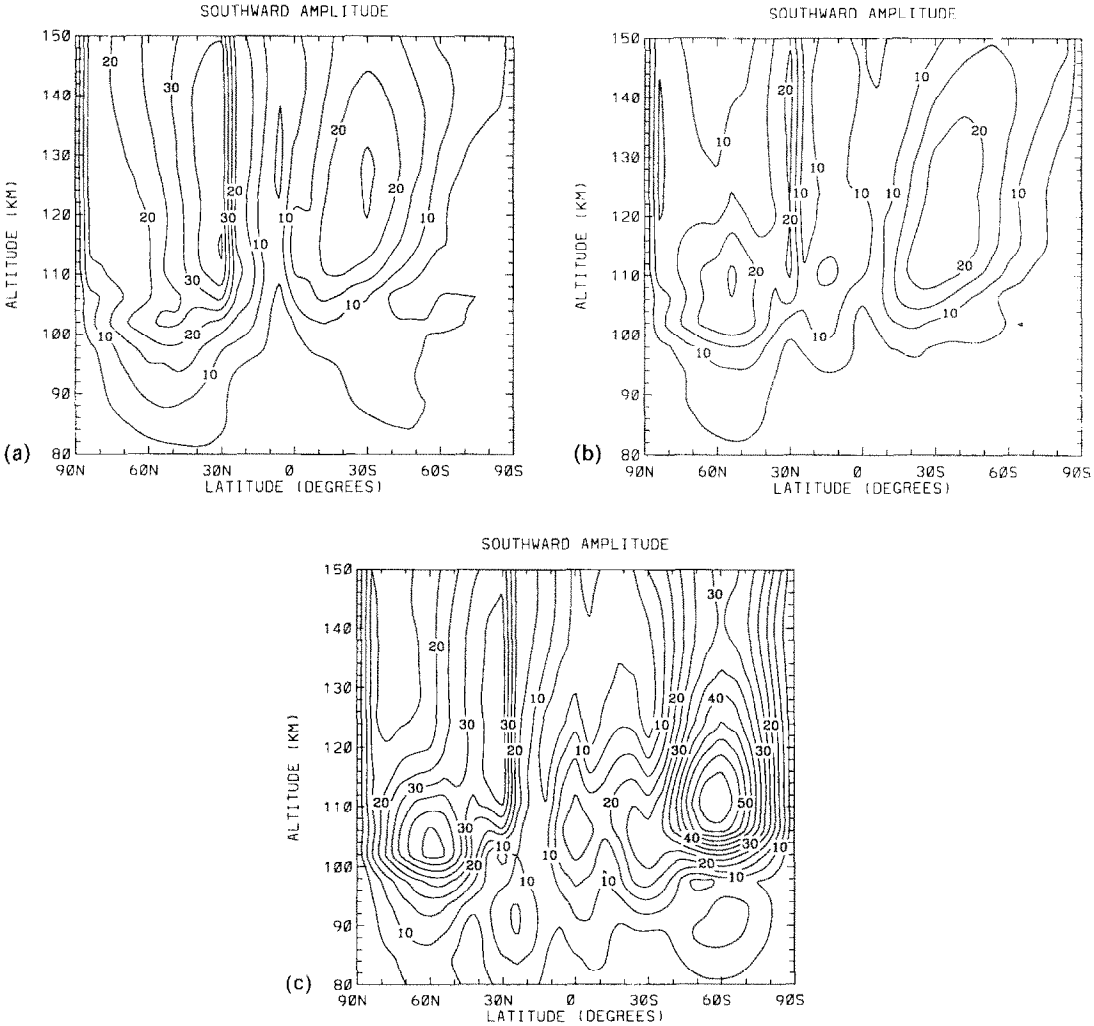


Fig. 8. Height vs. latitude contours for amplitude of the semidiurnal southward wind during December. Contour spacing is 5 m/s. (a) MLT data; (b) MLT and IS data; (c) FV89 model.

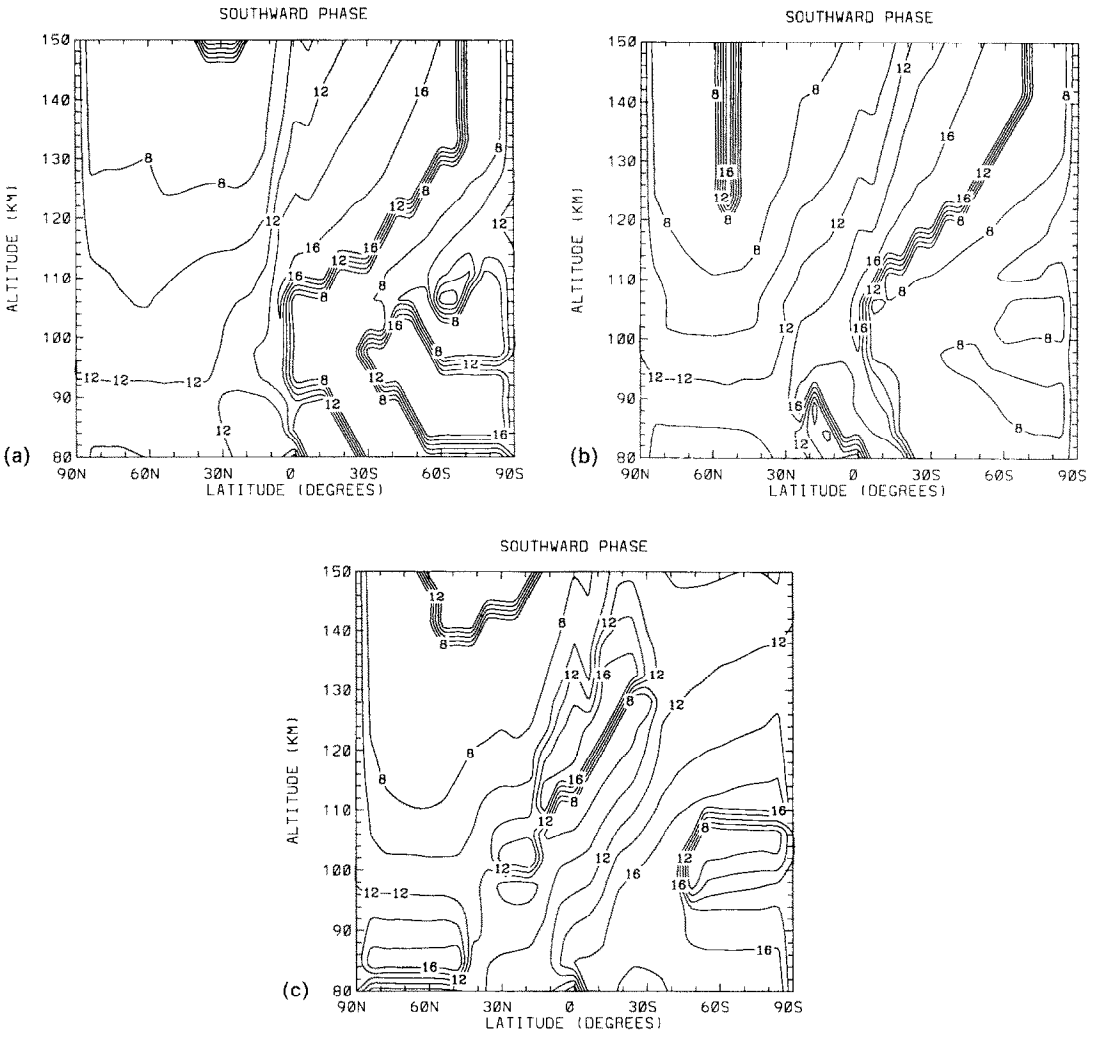


Fig. 9. Height vs. latitude contours for phase (local time of maximum) of the semidiurnal southward wind during December. Contour spacing is 2 h. (a) MLT data; (b) MLT and IS data; (c) FV89 model.

the data sources are provided in Table 1. Note that the Kyoto data were utilized in the fit, whereas the Atlanta data were not. In general, the salient features of the amplitude and phase variations of the Kyoto data are reflected in the MLTIS curve: amplitudes generally less than 8 m $s^{-1}$, and phases near 1900 (0700) LT, except for a shift to 0100–0200 (1300–1400) LT during midwinter. The main discrepancies occur during February, July and September for the amplitudes, and during March for the phases. One should bear in mind that on average the Kyoto station contributed measurements of eastward and southward winds at about seven different altitudes, or 14 'independent' data points for each monthly fit, out of a total of roughly 300–350 'independent' data points per month for all the stations combined. The FV89 amplitude curve provides nearly as good a representation of the Kyoto data as the MLTIS curve, on average, for both amplitudes and phases. Exceptions are the absence of an April/May amplitude maximum for FV89, and the relatively poor agreement for the FV89 phases during December–April. Similar considerations apply for the southward wind component illustrated in Fig. 11. The 'independent' data from Atlanta, however, show marked differences in many cases from the amplitude and phase curves for MLTIS and FV89, as well as the Kyoto data. The most striking differences occur during late winter and

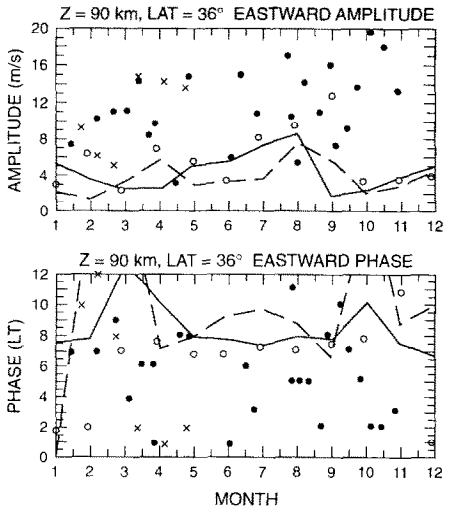


Fig. 10. Amplitude (top) and phase (bottom), expressed in hours from local midnight, of semidiurnal eastward wind component at 90 km altitude and 36° latitude. Solid line: FV89; dashed curve: MLTIS; open circles: Kyoto, Japan; closed circles: Atlanta, GA, 1984; crosses: Atlanta, GA, 1983.

spring, where the Atlanta amplitudes are at least a factor of two larger than the other values. Large amplitudes are also noted for the months around fall equinox, but this is not inconsistent with the rise in amplitude observed at Kyoto during the same part of the year. It is also during late winter and spring that the Atlanta phases deviate most from the general trends of MLTIS, FV89 and Kyoto. We do not understand completely the origin of these differences. In part, the larger amplitudes at Atlanta may be due to the shorter averaging interval; generally less than one month for a single year, whereas the data used in the fitting process usually represented monthly averages over several years at each station. This averaging tends to cancel out interannual differences and to reduce amplitudes. There may also be longitudinal differences in the tidal winds between Kyoto and Atlanta; the answer to this question awaits a comparative study of the two stations wherein the averaging intervals and data reduction methods have been made consistent.

A similar comparison is made in Figs 12 and 13, except for 52° latitude. Here the data compared with the MLTIS and FV89 curves consist of measurements from Saskatoon, Canada and Collm, Germany. The Saskatoon data were utilized in the fit, whereas the Collm data were not. The MLTIS curve tends to underestimate the Saskatoon amplitudes, especially during the late fall and winter months. The FV89 amplitude curves, in fact, appear to provide better representations of the Saskatoon data than the MLTIS curves generated from the fitting process. Neither MLTIS or FV89 show the large amplitudes in fall (usually September) that are generally characteristic of MLT radar tidal data over a wide range of middle latitudes (35–65°; Avery *et al.*, 1989; Manson *et al.*, 1989) (see also Figs 10 and 11). The generally smaller amplitudes derived from Collm are in better

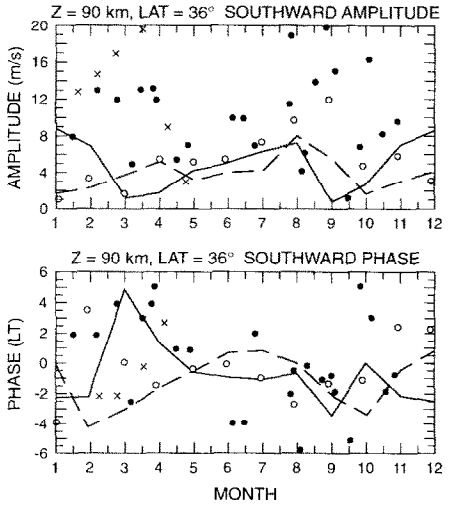


Fig. 11. Same as Fig. 10, except for southward component.

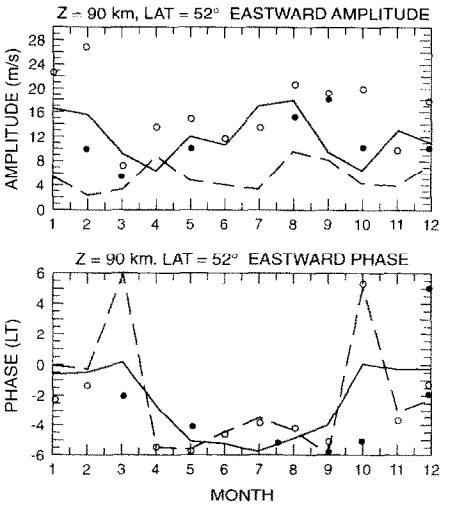


Fig. 12. Same as Fig. 10, except at 52° latitude. Open circles: Saskatoon, Canada; closed circles: Collm, Germany. The Collm data points are unequally spaced as they are obtained from the contours in Manson *et al.* (1989).

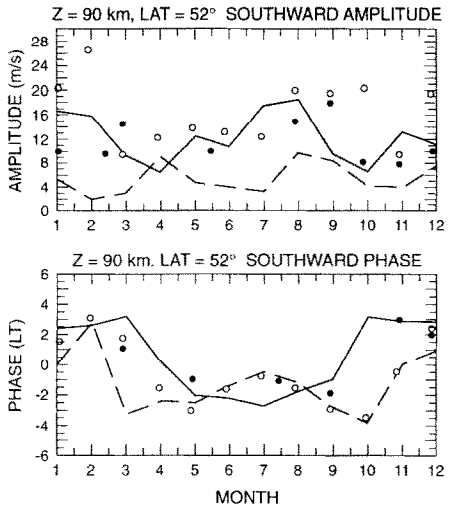


Fig. 13. Same as Fig. 12, except for southward component.

agreement with the FV89 and MLTIS curves. Again, to some degree, these differences may be related to the 1-yr averaging applicable to the Saskatoon data, as compared with the 3-yr averaging performed on the Collm data. The phases of both eastward and southward components, on the other hand, are in strikingly good agreement between both data sources and the MLTIS and FV89 curves.

## 5. CONCLUDING COMMENTS

Besides providing a forum for evaluation of a first-principles numerical model of atmospheric tides in the mesosphere and lower thermosphere, and adding confidence to our interpretation of the tidal dynamics of this atmospheric regime, the present study provides several useful purposes. First, the methodology developed here serves as a basis for the development of empirical models of tidal dynamics in the 80–150 km height regime. It is not insignificant that, although the data base consists primarily of wind measurements, the internal consistency of the HMEs also provides a prescription of the tidal oscillations in temperature, density, and pressure of the region, of which very few measurements exist. Density variations in particular are relevant for the prediction of re-entry drag on satellites, hypersonic vehicles and other aerospace applications. In addition, the analysis method presented here conveniently summarizes the global tidal data set in a form which enables the tidal oscillations at the lower boundary of Thermospheric GCMs (FESEN *et al.*, 1986) to be prescribed in a manner consistent with available observations.

Despite the excellent general agreement between FV89 and MLTIS, there are some important differences in the seasonal trends of amplitudes and phases, as demonstrated especially in Figs 10–13. This is consistent with the comparisons shown in AVERY *et al.* (1989), MANSON *et al.* (1989) and VINCENT *et al.* (1989). Some of these differences will be due to data inadequacies, e.g. different years, averaging, but some due to model limitations. It is desirable that HME reconstructions from MLTIS and FV89 be used by interested researchers to further explore the value of each product.

It is generally characteristic of the fitting process that amplitudes resulting from the fit are smaller than the majority of the observations going into the fit. This appears to be a consequence of attempting to simultaneously satisfy the various phase constraints imposed by the data. Phases, on the other hand, are reproduced with a higher degree of consistency. It is also striking that the phase structures are more nearly consistent with other model results and data. These points are evident from the comparisons between FV89 and MLTIS HME coefficients and tidal fields in Figs 1–4, and Figs 5–9, respectively, and between the MLTIS curves and data utilized in the fitting process as illustrated in Figs 10–13. Perhaps future uses of the present methodology specifically aimed towards empirical model development will address and improve upon the amplitude-suppressing aspect of the analysis method. From the point of view of interpreting the FV89 model results in the context of these observations, it must be considered that it is probably more appropriate to compare such a model with monthly averages within a given year, as opposed to a climatology over several years, at least in terms of making amplitude comparisons. Moreover, given the tendency for the fitting process to underestimate amplitudes, the comparatively larger values generally depicted in this paper for FV89 should not be prematurely viewed as a serious shortcoming of that model.

A shortcoming of the present analysis is that the monthly averages for the various stations do not cover the same time periods. The existence of interannual variability thus serves to make the comparisons less definitive than would be obtained from monthly averages constructed uniformly for all the radar sites. The fact that there are well-documented salient characteristics of the tidal structures which tend to repeat from year to year tends to ameliorate this shortcoming. In this context the present results may be viewed as 'interim' or 'preliminary', a more definitive study awaiting a data set with equally good geographical distribution, but representing averages over the same time periods. Given that key stations such

as Townsville, Garchy and Monpazier are no longer operating, and that newer ones are now emerging at other locations (Hawaii, Christmas Island), and recognizing the immense logistical effort in co-ordinating the formation of such a data base, it may be a considerable time before the present results become superseded.

*Acknowledgements*—The National Center for Atmospheric Research is sponsored by the National Science Foundation. This work was supported in part by Contract F19628-90-K-0014 from the U.S. Air Force Phillips Laboratory to Boston University. The authors are grateful to Mr Youngin Won of the University of Michigan for pointing out to us a numerical error in our original computations.

## REFERENCES


| | | |
|---|---|---|
| Avery S. K., Vincent R. A., Phillips A., Manson A. H. and Fraser G. J. | 1989 | *J. atmos. terr. Phys.* **51,** 595. |
| Fesen C. G., Dickinson R. E. and Roble R. G. | 1986 | *J. geophys. Res.* **91,** 4471. |
| Forbes J. M. | 1982a | *J. geophys. Res.* **87,** 5222. |
| Forbes J. M. | 1982b | *J. geophys. Res.* **87,** 5241. |
| Forbes J. M. and Hagan M. E. | 1982 | *J. geophys. Res.* **87,** 5253. |
| Forbes J. M. and Salah J. E. | 1991 | *J. geophys. Res.* **96,** 1135. |
| Forbes J. M. and Vial F. | 1989 | *J. atmos. terr. Phys.* **51,** 649. |
| Forbes J. M. and Vial F. | 1991 | *J. geophys. Res.* **96,** 1147. |
| Johnson R. M., Wickwar V. B., Roble R. G. and Luhmann J. G. | 1987 | *Ann. Geophys.* **A5,** 383. |
| Kazimirovsky E. S. and Zhovty E. I. | 1989 | *J. atmos. terr. Phys.* **51,** 683. |
| Labitzke K., Barnett J. J. and Edwards B. (eds) | 1985 | *Handbook for MAP* **16,** 318. |
| Manson A. H., Meek C. E., Teitelbaum H., Vial F., Schminder R., Kurschner D., Smith M. J., Fraser G. J. and Clark R. R. | 1989 | *J. atmos. terr. Phys.* **51,** 579. |
| Salah J. E., Wand R. H. and Bernard S. | 1977 | *Ann. Geophys.* **33,** 95. |
| Schminder R., Kurschner D., Manson A. H. and Meek C. E. | 1989 | *J. atmos. terr. Phys.* **51,** 623. |
| Vincent R. A., Tsuda T. and Kato S. | 1989 | *J. atmos. terr. Phys.* **51,** 609. |
| Wand R. H. | 1976 | *Radio Sci.* **11,** 641. |
| Wand R. H. | 1983a | *J. geophys. Res.* **88,** 7201. |
| Wand R. H. | 1983b | *J. geophys. Res.* **88,** 7211. |
| Wand R. H. | 1983c | *J. geophys. Res.* **88,** 9227. |
| Wand R. H. and Harper R. M. | 1978 | *J. atmos. terr. phys.* **40,** 887. |
| Wand R. H. and Salah J. E. | 1978 | *J. atmos. terr. Phys.* **40,** 913. |

*Reference is also made to the following unpublished material:*

| | | |
|---|---|---|
| Forbes J. M., Hagan M. E., Gillette D. F. and DiCesare E. | 1982 | AFGLK-TR-82-0173(II). |
| Lindzen R. S., Hong S.-S. and Forbes J. M. | 1977 | Mem. Rept 3442, Naval Res. Lab., Washington, D.C. |